VALDRIFT—A Valley Atmospheric Dispersion Model

K. JERRY ALLWINE

Allwine Environmental Services, Richland, Washington

XINDI BIAN AND C. DAVID WHITEMAN

Pacific Northwest National Laboratory, Richland, Washington

HAROLD W. THISTLE

USDA Forest Service, Missoula, Montana

(Manuscript received 25 April 1996, in final form 30 September 1996)

ABSTRACT

VALDRIFT (valley drift) is a valley atmospheric transport, diffusion, and deposition model. The model is phenomenological—that is, the dominant meteorological processes governing the behavior of the valley atmosphere are formulated explicitly in the model, although in a highly parameterized fashion. The key meteorological processes treated are 1) nonsteady and nonhomogeneous along-valley winds and turbulent diffusivities, 2) convective boundary layer growth, 3) inversion descent, and 4) nocturnal temperature inversion breakup. The model is applicable under relatively cloud-free, undisturbed synoptic conditions in which the winds in the valley are predominantly along the valley's axis. The model is configured to operate through one diurnal cycle for a single narrow valley. The inputs required are the valley topographic characteristics, pollutant release rate as a function of time and space, wind speed and direction as functions of time measured at one height, lateral and vertical turbulent eddy diffusivities as functions of stability, and the valley temperature inversion characteristics at sunrise. The outputs are three-dimensional concentration fields and ground-level deposition fields as functions of time. The scientific foundations of VALDRIFT are given in this paper along with a brief discussion of the model inputs and outputs. Air concentrations estimated by VALDRIFT compare favorably with results from a tracer experiment conducted in a deep mountain valley.

1. Introduction

Many population centers around the world are located in valleys, and air quality problems often occur when pollutant sources are located within or near the valleys (Hewson and Gill 1944; Tyson 1969; Wanner and Hertig 1984). Over the past two decades, numerous meteorological and tracer experiments have been conducted to investigate the dispersive characteristics of valley atmospheres (Start et al. 1975; Willson et al. 1983; Gryning and Lyck 1983; Gudiksen et al. 1984; Clements et al. 1989a; Whiteman 1989; Doran et al. 1990). Also, the dynamic and dispersive behavior of valley atmospheres has been investigated theoretically and with numerical models (McNider 1981; Bader and McKee 1985; Vergeiner et al. 1987; Segal et al. 1988; Bader and Whiteman 1989; Allwine 1992). These, and other such studies, have led to the identification of key physical processes governing dispersion in valleys, and a more complete understanding of these physical processes is emerging from ongoing research efforts. The important physical processes include up- and down-valley winds, up- and downslope winds, turbulent diffusion, convective boundary layer growth, temperature inversion descent, nocturnal temperature inversion breakup, tributary flows, cross-valley circulations, subsidence, and interactions with above-ridge-top winds.

These physical processes, in addition to source characteristics, chemical transformations, and deposition, should be included in valley air quality models to properly simulate the transport and fate of atmospheric releases. An effective approach for treating the important processes in models is to describe each physical process explicitly in terms of empirical, semiempirical, or theoretical relationships—that is, to use algebraic or simple numerical relationships to represent each important process. The alternative approach is to solve the coupled conservation equations of mass, momentum, and energy with appropriate initial and boundary equations. Currently, the most reasonable approach for ''applications'' models is the phenomenological modeling approach

Corresponding author address: Dr. K. Jerry Allwine, Allwine Environmental Services, 1763 Duluth Street, Richland, WA 99352.
E-mail: jallwine@owt.com

since applications models based on the ''first-principles'' approach are generally still too complicated for release to, and routine use by, the general user community.

A project initiated by the U.S. Forest Service in 1990 (Ekblad and Barry 1990) led to the development of VALDRIFT (valley drift), a model that is well suited for estimating the drift of pesticides from aerial spraying operations that are usually conducted in the morning hours after first light, under relatively cloud-free, undisturbed synoptic conditions (Ekblad et al. 1991). The spraying generally continues until convective boundary layers and upslope flows develop sufficiently to render it difficult to place the spray where needed in the canopy (Whiteman 1990). On an undisturbed clear day, the spraying is generally terminated in mid- to late morning. VALDRIFT can be used to estimate the drift of pesticide that does not deposit to the canopy, where the pesticide mass remaining in the air can be estimated from existing aerial pesticide spray models (Bilanin et al. 1989; Teske et al. 1993).

This paper describes the phenomenological air quality model VALDRIFT, where the dominant physical processes governing atmospheric transport and diffusion are treated explicitly in the model in a highly parameterized fashion. Section 2 of this paper discusses the basic foundations of the VALDRIFT model, section 3 compares VALDRIFT with tracer data collected in a deep mountain valley, and section 4 gives the summary and conclusions.

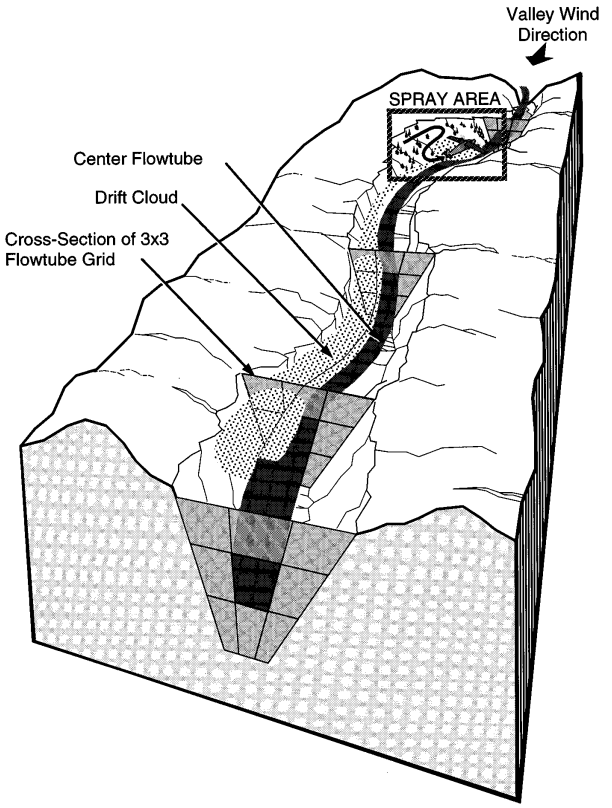

FIG. 1. Example of the flowtube approach used in VALDRIFT.

2. Model formulation

a. Overview

VALDRIFT treats the transport, diffusion, and deposition of an inert substance released from multiple point and/or line sources in a valley atmosphere, where the sources may be elevated or at ground level and the release rate from each source can vary with time. The released substances can be either gases or aerosols having negligible settling velocities. VALDRIFT is configured to simulate one diurnal cycle for a single relatively narrow mountain valley having relatively steep sidewalls (sidewall angles of 10°–90°). The inputs required are the valley topographic characteristics, pollutant release rate as a function of time and space, wind speed and direction as functions of time measured at one height, lateral and vertical turbulent eddy diffusivities as functions of stability, and the valley temperature inversion characteristics at sunrise. The outputs are three-dimensional concentration fields and ground-level deposition fields as functions of time. VALDRIFT is written in standard Fortran and can be run on any computer system with the appropriate Fortran compiler. Execution times are roughly 2–3 min per hour of simulation time on a 486-level personal computer.

The physical processes currently treated explicitly in VALDRIFT are nonsteady and nonhomogeneous along-valley winds and turbulent diffusivities, convective boundary layer growth, inversion descent, and nocturnal temperature inversion breakup. Slope flows, cross-valley circulations, interactions with above-ridge-top winds, subsidence, nocturnal temperature inversion formation, and tributary flows are not currently treated in VALDRIFT. The model is applicable under relatively cloud-free, undisturbed synoptic conditions in which the diurnal evolution of the surface sensible heat flux drives the formation and behavior of the valley winds. The winds in the valley are predominantly along the valley's axis.

A more detailed technical description of VALDRIFT and operating instructions for the model are given in the VALDRIFT user's guide (Allwine et al. 1995).

b. Computational grid

The basic computational approach in VALDRIFT is to solve a one-dimensional (along-valley) species conservation equation for each of a number of ''flowtubes'' aligned along the valley, as illustrated in Fig. 1. Figure 1 shows a section of valley divided into nine flowtubes. The flowtube in the center of the valley is outlined to show its conformity with the shape of the valley.

The computational domain should extend far enough

down-valley and up-valley from the pollutant release area to handle transport distances commensurate with the simulation period. This could be up to 100 km up-valley and down-valley (provided that the valley is this long) for one diurnal cycle, depending on the strength of the along-valley flows. Another consideration is that the domain must extend far enough beyond the receptor area of concern that edge effects are minimized. That is, material advected off the grid is lost and, consequently, cannot contribute to concentrations inside the model domain in the event of flow reversal. The cross-valley extent of the domain should be from ridge top to ridge top.

The VALDRIFT coordinate system (*S*, *Y*, and *Z*) is nonorthogonal, with the *S* axis following the valley floor centerline in the down-valley direction. The origin is at the up-valley edge of the domain at the center of the valley cross section on the valley floor. The positive *S* axis points down the valley axis at the valley center, the positive *Y* axis extends horizontally to the right (looking up-valley), locally perpendicular to the *S* axis, and the positive *Z* axis is oriented vertically. The rigorous transformation of the species conservation equation from a Cartesian (rectangular) coordinate system into the ''valley-following'' coordinate system used by VALDRIFT would theoretically introduce ''stretching factors'' into the transformed equation. These stretching factors, however, are not included in the species conservation equation in order to maintain computational efficiency. The errors introduced into the solution are small for valleys that do not change course by more than approximately 45° within a few kilometers.

Once the computational domain has been determined, certain terrain characteristics need to be specified. These can be determined from contour maps and/or computer-based digital elevation datasets. The terrain characteristics required at various valley cross sections are S_{xc} the down-valley distance of the cross section (m), α_L the left sidewall angle (degrees), α_R the right sidewall angle (degrees), z_f the elevation of the valley floor (m MSL), z_r the elevation of the ridge tops (m MSL; if the ridge-top elevations differ for the two sidewalls, use the lower of the two elevations), and *l* the width of the valley floor (m). The number of cross sections can range from one to several, depending on the variability in the shape of the valley. The terrain characteristics of a valley cross section should be specified wherever significant changes occur in the valley shape. Each valley cross section is represented as shown in Fig. 2.

The computational grid is generated by specifying the number of flowtubes in the cross-valley and vertical directions—for example, 3 × 3, as shown in Fig. 1. An initial cross section is divided into the desired number of layers in the vertical direction, and each layer is divided into the desired number of flowtubes in the cross-valley direction. This initial cross section should be ''typical'' and roughly the median in the cross-sectional area. The entire grid is generated using the conditions that the flowtubes are always horizontal in the cross-valley direction, are conformal to the valley sidewalls in the vertical direction, and the ratio of the cross-sectional area of each flowtube to the total cross-sectional area of the valley does not vary in the along-valley direction.

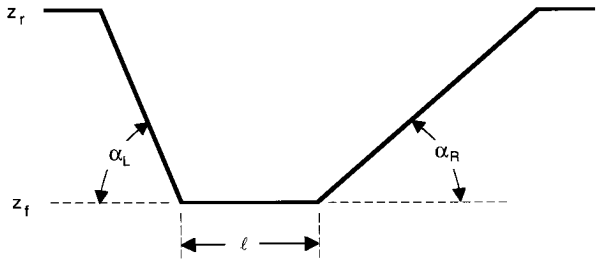

FIG. 2. Simplified valley cross section showing required parameters.

c. Dispersion model

Interactions among flowtubes can occur and are handled through source–sink terms in the species conservation equation for each flowtube. The species conservation equation, to be solved for each flowtube, is

$$\frac{\partial(AC)}{\partial t} + \frac{\partial(\dot{V}C)}{\partial S} - \Gamma_{cs} - \Gamma_{cp} - \Gamma_{cd} = 0, \qquad (1)$$

where the first term is the rate of change of the storage of *C* in the differential control volume *AdS*, the second term is the along-valley advection of *C*, *t* is time (s), *S* is the along-valley coordinate (m), *C* is the concentration along the flowtube (g m^{-3}), *A* is the cross-sectional area of the flowtube (m^2) and is a function of *S*, $\dot{V}$ is the along-valley air volume flow rate through the flowtube (m^3 s^{-1}), Γ_{cs} is the emission source–sink term for the flowtube, Γ_{cp} is the deposition source–sink term, and Γ_{cd} is the turbulent diffusion source–sink term. All source–sink terms have units of grams per second per meter. VALDRIFT does not currently treat chemical transformations or lateral and vertical advection.

The conservation of species equation (1) for each flowtube is integrated using a fully explicit finite-difference scheme consisting of forward Euler differencing in time, upwind differencing for advection, and central differencing for diffusion. Concentration initial conditions and boundary conditions are required to solve (1). The initial conditions are that the concentrations are constant for all *S*, where the constant value is specified by the user. The choice of boundary conditions in VALDRIFT is either of the Dirichlet type, where *C* is specified (same value as the initial conditions), or of the von Neumann type, where the gradient of *C* is specified. VALDRIFT only allows a zero gradient boundary condition (i.e., the inflow concentration is set equal to the concentration in the first downwind grid cell) if the von Neumann type of boundary condition is selected.

Equation (1) is solved for each flowtube, where the number of grid cells in the along-valley direction (S coordinate) is specified by the user. A typical VALDRIFT computational grid would be 100 grid cells in the along-valley direction by 10 cells in each of the cross-valley (Y coordinate) and vertical (Z coordinate) directions.

1) EMISSION SOURCE–SINK TERM Γ_{cs}

The emission source–sink term is simply the rate of pollutant mass released to each grid cell per unit length of the grid cell during a model time step. Most grid cells in the modeling domain will probably have Γ_{cs} equal to zero. VALDRIFT maps releases from all point and line (flight paths) sources specified by the user to the appropriate grid cells. The release data required are the coordinates of each point source, the beginning and ending time of the release from each point source, the total mass of pollutant released from each point source, the coordinates of the starting and ending location of each line source (flight path), the beginning and ending times of the release from each line source, and the total mass of pollutant released from each line source.

2) DEPOSITION SOURCE–SINK TERM Γ_{cp}

The deposition source–sink term in VALDRIFT currently treats only dry deposition using a source depletion model (see, e.g., Hanna et al. 1982). The dry deposition parameterization is given by the equation

$$\Gamma_{cp} = V_d C_d \frac{\Delta A}{\Delta S}, \tag{2}$$

where V_d is the dry deposition velocity (m s^{-1}) specified by the user, C_d is the concentration in a grid cell adjacent to the ground (g m^{-3}), ΔA is the ground surface area of the grid cell (m^2), and ΔS is the along-valley length of the grid cell (m).

The amount of pollutant deposited to the ground at a grid cell adjacent to the ground is determined as

$$\omega_d = V_d C_d \Delta t, \tag{3}$$

where ω_d is the mass deposited to the ground (g m^{-2}) during a model time step Δt (s).

3) TURBULENT DIFFUSION SOURCE–SINK TERM Γ_{cd}

Material can move among flowtubes by turbulent diffusion. The turbulent diffusion source–sink term represents the amount of material added or removed from a grid cell because of turbulent diffusion, where the turbulent diffusion is described using K theory. The source–sink term representing diffusion in (1) is given as

$$\Gamma_{cd} = \Gamma_{cdY} + \Gamma_{cdZ}, \tag{4}$$

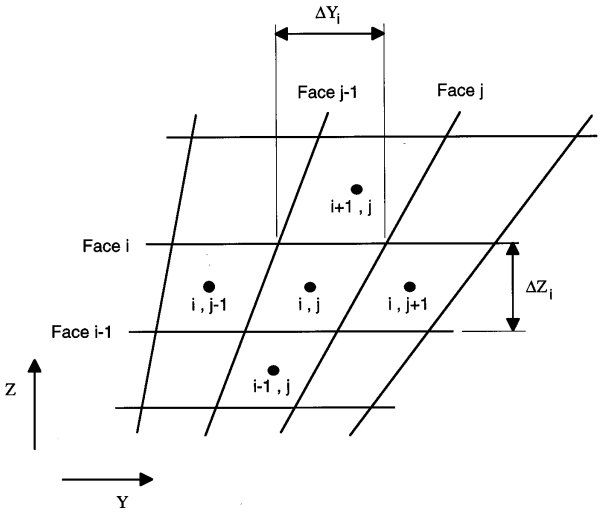

FIG. 3. Index notation associated with the flowtubes on a valley cross section.

where the lateral and vertical turbulent diffusion terms are represented by

$$\Gamma_{cdY} = \overline{\dot{V}'_Y C'}\big|_{\text{face}j} - \overline{\dot{V}'_Y C'}\big|_{\text{face}j-1} \tag{5}$$

and

$$\Gamma_{cdZ} = \overline{\dot{V}'_Z C'}\big|_{\text{face}i} - \overline{\dot{V}'_Z C'}\big|_{\text{face}i-1}, \tag{6}$$

and the overbar terms represent the time-averaged turbulent fluxes of C in the Y and Z directions, as denoted, where Y is the cross-valley coordinate. The turbulent volume flow terms ($\dot{V}'_Y$ and $\dot{Y}'_Z$) are flow in the Y and Z directions per unit length in the S direction (m^3 s^{-1} m^{-1}). The i index refers to the vertical direction, and the j index refers to the lateral direction. The index notation for a subset of flowtubes on a valley cross section is shown in Fig. 3. The lateral and vertical diffusion source–sink terms evaluated using (5) and (6), respectively, represent the i, j computational grid cell. Equations (5) and (6) are approximated using K theory as

$$\Gamma_{cdY} = \Delta Z_i K_{Y,i} \frac{\partial C}{\partial Y}\bigg|_{\text{face}j} - \Delta Z_i K_{Y,i} \frac{\partial C}{\partial Y}\bigg|_{\text{face}j-1} \tag{7}$$

and

$$\Gamma_{cdZ} = \Delta Y_i K_{Z,i} \frac{\partial C}{\partial Z}\bigg|_{\text{face}i} - \Delta Y_{i-1} K_{Z,i-1} \frac{\partial C}{\partial Z}\bigg|_{\text{face}i-1}, \tag{8}$$

where K_Y is the lateral turbulent eddy diffusivity and K_Z is the vertical turbulent eddy diffusivity, which are both functions of atmospheric stability and are specified by the user. The lengths ΔY and ΔZ are functions only of Z on each cross section and are determined from the characteristics of the computational grid. The derivatives in (7) and (8) are evaluated in VALDRIFT using central finite differencing.

In the current VALDRIFT formulation, diffusion in the along-valley direction is assumed to be negligible

relative to the along-valley advection, and consequently, the *S*-direction diffusion source–sink term is set equal to zero.

d. Meteorological model

The meteorological inputs needed to determine the pollutant concentration from (1) are the wind speed and direction as functions of time at one height, the nocturnal temperature inversion characteristics at sunrise, the heating rate of the valley atmosphere after sunrise, and the turbulent eddy diffusivities as functions of atmospheric stability. The wind speed and direction observations at one height are used to determine the along-valley air volume flow rates used in the advection term in (1). The nocturnal temperature inversion characteristics at sunrise and the heating rate of the valley atmosphere determine the evolution of the convective boundary layer (CBL) and inversion-top descent during the morning transition period. The locations of the top of the CBL and the top of the temperature inversion define layers with different atmospheric stabilities—unstable within the CBL, stable between the top of the CBL and the top of the inversion, and neutral above the top of the inversion. Different turbulent eddy diffusivities are used in (7) and (8) to determine the diffusion source–sink term in (1), depending on the stability region coincident with the computational grid cell.

This section gives the basic formulations for determining the along-valley air volume flow rates in the valley and the breakup of the nocturnal temperature inversion during the morning transition period. A brief discussion of recommended values of lateral and vertical turbulent eddy diffusivities then follows.

1) ALONG-VALLEY FLOWS

Assuming the flow to be incompressible, the air mass (volume) in the valley is conserved following the equation

$$\frac{\partial \dot{V}(S, t)}{\partial S} - \Gamma_a(S, t) = 0, \tag{9}$$

where $\dot{V}$ is the total along-valley volume flow rate ($m^3\ s^{-1}$) and Γ_a is the airmass source–sink term ($m^3\ s^{-1}\ m^{-1}$). Possible sources and sinks of air mass are from subsidence, regional flow intrusions, and tributary flows. The air mass is also conserved for each flowtube, *ij*, following the equation

$$\frac{\partial \dot{V}_{ij}(S, t)}{\partial S} - \Gamma_{a,ij}(S, t) = 0, \tag{10}$$

where $\dot{V}_{ij}$ is the along-valley volume flow rate in flowtube *ij* ($m^3\ s^{-1}$) and $\Gamma_{a,ij}$ is the airmass source–sink term in flowtube *ij*. Integrating (10) between a starting cross section, S_0, and some arbitrary cross section, *S*, gives

$$\dot{V}_{ij}(S, t) = \dot{V}_{ij}(S_0, t) - \int_{S_0}^{S} \Gamma_{a,ij}(S', t)\, dS'. \tag{11}$$

Therefore, given the volume flow rate at S_0 and the source–sink terms for all *S*, the volume flow rate for each flowtube at time *t* can be determined for all *S* from (11). The volume flow rate for each *ij* flowtube at S_0 is determined as

$$\dot{V}_{ij}(S_0, t) = u_{ij}(S_0, t)\, A_{ij}(S_0), \tag{12}$$

where u_{ij} is the average along-valley wind speed in flowtube *ij* and A_{ij} is the cross-sectional area of flowtube *ij*. Currently all airmass source–sink terms in VALDRIFT are set to zero; no sources or sinks of air are treated.

The along-valley winds in a deep mountain valley typically take the form of a jet, with the peak winds above the valley floor centered between the two sidewalls. The winds decrease to zero at the valley sidewalls, the valley floor, and at a height near the ridge tops. Clements et al. (1989b) describe the cross-valley and vertical structure of the along-valley winds $u(Y, Z, t)$ using a semiempirical relationship called a ''Prandtl parabolic wind profile'':

$$u(Y, Z, t) = U(t)\left\{0.95 - 0.85\left[\frac{Y}{W(Z)}\right]^2\right\} \times \left[3.2 \exp\left(-\frac{3.3Z}{D}\right) \sin\left(\pi\frac{Z}{D}\right)\right], \tag{13}$$

where $U(t)$ is the jet maximum along-valley wind speed as a function of time, *W* is the valley half-width (m), and *D* is the depth of the drainage flow above the valley floor (height at which wind speed goes to zero) and is assumed to extend to the ridge tops. Equation (13) fully describes the along-valley winds provided $U(t)$ is known; $U(t)$ is determined as

$$U(t) = u(0, Z_1, t)\left\{0.95\left[3.2 \exp\left(-\frac{3.3Z_1}{D}\right) \sin\left(\pi\frac{Z_1}{D}\right)\right]\right\}^{-1}, \tag{14}$$

where $u(0, Z_1, t)$ is the along-valley component of the wind observed at the center of the valley ($Y = 0$) at one height above the valley floor ($Z = Z_1$). Once $U(t)$ is known, $u(Y, Z, t)$ from (13) can be integrated over the area of flowtube *ij* to determine the u_{ij} used in (12). The along-valley wind component as a function of time, $u(0, Z_1, t)$, is determined from the wind speed and direction observations at height Z_1, and the down-valley direction of the valley axis at the wind observation site. The observed wind vector at each observation time is resolved into along-valley and cross-valley components, and then the along-valley component is used in (14). The along-valley wind speeds are positive in the down-valley direction and negative in the up-valley direction.

2) CBL GROWTH AND INVERSION DESCENT

The morning transition period is the postsunrise period when the nocturnal down-valley flow is reversed to up-valley flow and when the nocturnal temperature inversion descends in the valley and is destroyed by the growth of a convective boundary layer. The approach for treating the morning transition period in VALDRIFT is based on the CBL growth–inversion descent thermodynamic model developed by Whiteman and McKee (1982) and implemented by Whiteman and Allwine (1985) in their valley dispersion model VALMET (valley meteorology).

The heat flux that destroys a nocturnal temperature inversion is distributed quite differently in a valley than over homogeneous terrain. Over homogeneous terrain, the sensible heat flux destroys the inversion by driving the upward growth from the ground of a convective boundary layer, which warms the inversion air mass from below until the temperature deficit is overcome and the inversion is destroyed. In a valley, the upward heat flux also develops a CBL over valley surfaces, but in contrast, the heated slopes cause warmed air parcels to flow upslope. These upslope flows remove mass from the base of the temperature inversion and, through mass continuity, result in a general subsiding motion over the valley center. The atmospheric energy budget approach used by Whiteman and McKee (1982) is capable of partitioning energy between these two different processes to produce inversion destruction solely by CBL growth, solely by inversion descent (assuming that a nongrowing CBL is present initially in a simulation), or by a combination of the two processes. The partitioning is controlled by a single parameter, f_C, defined as the fraction of sensible heat flux going to CBL growth. The remaining fraction, $1 - f_C$, is assumed to be responsible for mass transport up the valley sidewalls, which results in inversion descent.

The thermodynamic model is composed of two coupled equations. The first equation is a prediction equation for CBL height in which, in accordance with the bulk nature of the model, the CBL depth H_C is assumed not to differ over the valley floor and sidewalls. The first equation is

$$H_{C,n} = H_{C,n-1} + \Delta H_{C,n-1}, \qquad N_{tsr} < n \le N_{tss}, \quad (15)$$

where

$$\Delta H_{C,n-1} = \frac{\theta}{T}\frac{f_C}{\rho c_p}\frac{l + \Theta H_{C,n-1}}{l + \Theta(H_{C,n-1}/2)}\frac{A_0 A_1}{\gamma_\theta H_{C,n-1}} \times \sin\left[\frac{\pi}{\tau}\Delta t(n - N_{tsr})\right]\Delta t, \quad (16)$$

$$\frac{\theta}{T} = \left(\frac{1000}{P}\right)^{0.286}, \quad (17)$$

and P is the atmospheric pressure (mb), ρ is the density of the air in the valley atmosphere (kg m^{-3}), c_p is the specific heat of air at constant pressure (1005 m^2 K^{-1} s^{-2}), A_0 is the fraction of extraterrestrial solar flux that is partitioned to sensible heat flux ($0 < A_0 < 1$), A_1 is the extraterrestrial solar flux on a horizontal surface at solar noon (W m^{-2}), γ_θ is the valley potential temperature lapse rate at sunrise (K m^{-1}), τ is the length of the daylight period (s), N_{tsr} is the time step of sunrise, N_{tss} is the time step of sunset, l is the width of the valley floor (m), and Θ is $\cot\alpha_L + \cot\alpha_R$. Note that a nonzero initial CBL height is necessary to make (16) tractable. In the model, this requirement is met by using an initial CBL height at sunrise of 25 m. The second equation describing the height of the inversion-top h_I is

$$h_{I,n} = h_{I,n-1} + \Delta h_{I,n-1}, \qquad N_{tsr} < n \le N_{tss}, \quad (18)$$

where

$$\Delta h_{I,n-1} = \frac{(\beta_w/2)(h_{I,N_{tsr}} - h_{I,n-1})[l + \Theta(h_{I,N_{tsr}} - h_{I,n-1})/2]}{h_{I,n-1}\gamma_\theta(l + \Theta h_{I,n-1}/2) - \Delta t(n - N_{tsr})(\beta_w/2)(l + \Theta h_{I,n-1})}\Delta t - \frac{\theta}{T}\frac{1}{\rho c_p}\frac{[(l + \Theta h_{I,n-1}) - f_c(l + \Theta H_{I,n-1})]A_0 A_1 \sin\left[\frac{\pi}{\tau}\Delta t(n - N_{tsr})\right]}{h_{I,n-1}\gamma_\theta(l + \Theta h_{I,n-1}/2) - \Delta t(n - N_{tsr})(\beta_w/2)(l + \Theta h_{I,n-1})}\Delta t \quad (19)$$

and β_w is the warm-air advection rate above the valley (K s^{-1}).

The numerical simulation using the coupled equations (15) and (18) proceeds with discrete time steps and is completed when the inversion is destroyed at the first time step for which $H_{c,n} \ge h_{I,n}$—that is, for which the CBL height becomes greater than the inversion-top height.

The terms in (19) involving the warming rate for the air above the inversion allow the model to incorporate the retarding effect on temperature inversion breakup caused by warm air advection above the valley temperature inversion. Extra energy is required to destroy the valley temperature inversion if this warming occurs during the temperature inversion breakup period be-

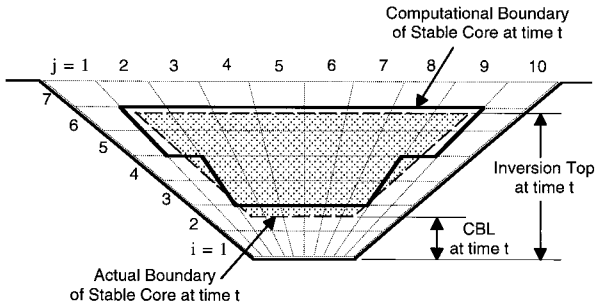

FIG. 4. Illustration of the computational domain on a valley cross section at time t after sunrise. The stable core (stippled area), CBL height, and inversion-top height are shown within a 7×10 array of valley flowtubes.

cause the inversion cannot be broken until the entire valley atmosphere is warmed to the temperature of the air above the valley.

The time of sunrise, time of sunset, length of the daylight period, and the solar flux at solar noon used in (16) and (19) are calculated using Whiteman and Allwine's (1986) solar model, given the latitude and longitude of the center of the modeling region and the month, day, and year of the simulation.

In summary, the parameters needed by VALDRIFT to treat CBL growth–inversion descent are the fraction of sensible heat flux going to CBL growth f_C, the atmospheric pressure P, the density of the air in the valley atmosphere ρ, the fraction of extraterrestrial solar flux that is partitioned to sensible heat flux A_0, the valley potential temperature lapse rate at sunrise γ_θ, and the warm-air advection rate above the valley β_w.

3) TURBULENT EDDY DIFFUSIVITIES

In VALDRIFT, lateral and vertical turbulent eddy diffusivities (K_Y and K_Z) are assigned according to three locally specified regimes—stable, neutral, and unstable. The valley atmosphere is assumed stable during the nighttime and within the ''stable core'' during the morning transition period. In the region above the stable core during the morning transition period, the valley atmosphere is assumed to be neutral, and within the growing CBL, the valley atmosphere is considered unstable. After the nocturnal temperature inversion has been destroyed and the stable core is no longer present, the valley atmosphere is considered to be unstable until sunset. After sunset, the valley atmosphere is assumed to be stable again.

The representation of the stable core region by the VALDRIFT computation grid is shown in Fig. 4. When the CBL grows above the center of a flowtube, the flowtube is assumed to be fully contained within the CBL. The same approach applies to the inversion descent, where the flowtube is fully contained in the flows above the inversion top once the inversion top descends below the center of the flowtube. The determination of which turbulent diffusivities apply to which flowtube depends on the flowtube's location relative to the stable core. For example, the first two rows ($i = 1$ and 2) of flowtubes in Fig. 4 would be assigned unstable diffusivities because they are contained in the CBL, and the diffusivities for the top row ($i = 7$) of flowtubes would be based on neutral stability.

The lateral and vertical turbulent eddy diffusivities are provided as input to VALDRIFT. Appropriate values of K_Y and K_Z are, however, typically not available, especially for complex terrain environments. The best approach for determining appropriate diffusivity values is to measure K_Y and K_Z for the valley of interest, but these measurements are rarely made. An alternate approach is to approximate K_Y and K_Z using existing turbulence theory formulations such as, for example, the formulations described by Businger et al. (1971) and Panofsky and Dutton (1984). Typical daytime (unstable) values of K_Z are on the order of 10 $m^2\ s^{-1}$, with nighttime (stable) values being typically less that 1 $m^2\ s^{-1}$. Values of K_Y range from roughly 6 times the K_Z value for stable conditions to roughly 1.5 times the K_Z value for unstable conditions.

3. Comparison with tracer data

a. Description of data

The VALDRIFT model was compared with tracer data from an experiment conducted in Colorado's Brush Creek–Roan Creek (BCRC) valley system on 26 September 1984 (Clements et al. 1989a). This experiment was conducted as part of the Department of Energy's (DOE's) Atmospheric Studies in Complex Terrain (ASCOT) research program. The 26 September experiment was one of several tracer and meteorological experiments conducted during September and October 1984. Three nonreactive, gaseous, perfluorocarbon tracers were released simultaneously during each experiment. Tracer concentrations were measured at more than 90 locations at ground level, and 11 locations were measured with vertical profiling instruments. Allwine (1993) gives a detailed analysis of the 26 September tracer experiment.

A subset of the results from the 26 September perfluoromethylcyclohexane (PMCH) tracer release was compared with VALDRIFT. On this date, the PMCH was released at a nearly constant rate of 0.23 g s^{-1} at a height of 5 m above the valley floor, with the release starting at midnight and terminating at 0900 LST (when winds switched from down-valley to up-valley). Ground-level and elevated tracer samples were collected starting at midnight and continuing through 1000 LST, with some samplers collecting until noon.

Evaluating VALDRIFT's ability to predict ground-level concentrations at the valley center is the scope of this analysis. Thus, VALDRIFT was compared with hourly integrated PMCH concentrations measured at

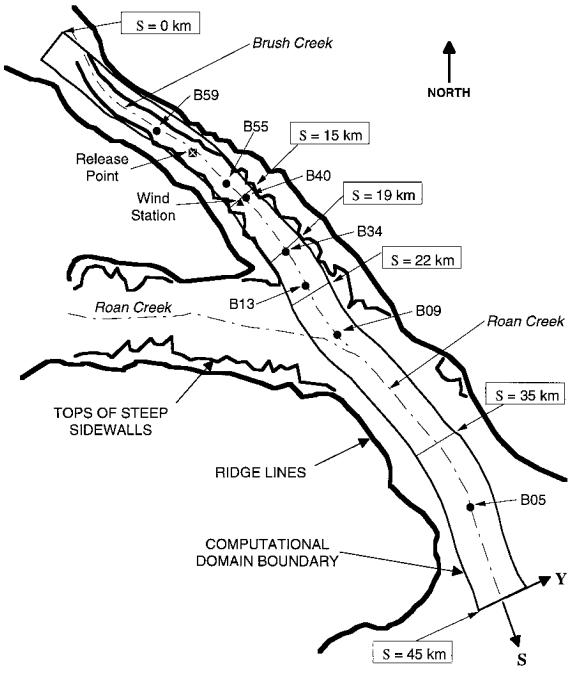

FIG. 5. Computational domain for the Brush Creek valley simulation. Terrain characteristics are specified in VALDRIFT at the six locations identified by the ''boxed'' text. The locations of the tracer release (⊠), wind station (▲), and seven tracer samplers (●) are identified.

seven ground-level locations at which air samples were collected from midnight to 1000 LST. The cross-valley and elevated concentration results from VALDRIFT could also be evaluated later by using all the ground-level and elevated tracer sampling results from the 26 September 1984 ASCOT experiment.

Figure 5 gives a schematic of the BCRC valley system showing the PMCH release location and the sites of the seven ground-level tracer samplers used in the comparison with VALDRIFT. The tracer samplers B59, B55, B40, B34, B13, B09, and B05 are located at the center of the valley at down-valley coordinate S and are of 8.5, 13.5, 15, 19, 21, 25, and 39 km, respectively. Samplers B59, B55, B40, and B34 are located in the Brush Creek valley, and samplers B13, B09 and B05 are in the Roan Creek valley, down-valley from the Brush Creek–Roan Creek confluence. The release is located in the Brush Creek valley at S equal to 11 km.

Winds were measured continuously during the 26 September ASCOT experiment at several locations in the BCRC valley system using various instruments, including tethersondes and Doppler sodars. VALDRIFT requires wind speed and direction observations as functions of time at one height in the valley, so 15-min-average observations from one height from a Doppler sodar located in the Brush Creek valley at S equal to 15 km (Fig. 5) were used as input to VALDRIFT. The along-valley winds that developed in the BCRC valley system were adequately represented by the Prandtl parabolic wind profile given by (13) and were not significantly influenced by the partial cloud cover and 3–5 m s^{-1} above-ridge-top winds experienced on 26 September.

TABLE 1. Terrain characteristics at six cross sections in Brush Creek valley.

S_{xc} (km)	z_r (m MSL)	z_f (m MSL)	α_L (°)	α_R (°)	l (m)
0	2550	1900	36	36	300
15	2550	1900	36	36	300
19	2510	1840	36	36	450
22	2480	1795	36	36	750
35	2450	1650	36	36	800
45	2400	1550	36	36	850

b. Model setup

The VALDRIFT simulation start and stop times were 0000 LST and 1200 LST, respectively, on 26 September 1984, and the number of grid cells in the *S, Y,* and *Z* directions were 100, 7, and 7. The length of the BCRC valley computational domain was 45 km, as shown in Fig. 5. The BCRC valley coordinates of 39.5°N, 108.4°W gave a solar noon extraterrestrial solar flux of 1030 W m^{-2}, and sunrise and sunset times on the ridge tops of 0610 and 1800 LST.

The shape of the BCRC valley was represented in VALDRIFT by the six idealized valley cross sections specified at the locations shown in Fig. 5. Table 1 gives the terrain characteristics of the six cross sections. Interestingly, the average sidewall angles at the cross sections were estimated to all be the same, about 36°, on both sides of the valley.

Doppler sodar wind speed and direction observations as functions of time at the height of the jet maximum winds (105 m above the valley floor) were input to VALDRIFT. It should be noted, however, that the maximum winds at the height of the jet peak are not required, but should be used in VALDRIFT if available. Additional model inputs required to determine the along-valley volume flows were the *S* coordinate of the wind station (15 km), the down-valley direction at the wind station (140°, the azimuth angle relative to 0°N, toward which the down-valley direction points), the height of the observations (105 m), the frequency of the data (15 min), and the year-month-day-hour-minute (84-09-26-00-00) of the first record.

The turbulent eddy diffusivities used in the BCRC valley simulation were estimated using surface-layer turbulence parameterizations of Businger et al. (1971) and Panofsky and Dutton (1984). The basic philosophy in developing the VALDRIFT scheme was that, since the wind profile in the valley is jet shaped, surface-layer scaling could be used to determine the diffusivities representative of the entire valley atmosphere. The diffusivities are determined at a ''reference'' height of 0.2

times the height of the jet wind maximum, where the reference height is within the surface layer for most valleys (valleys with the height of the jet maximum below 250 m). From the Prandtl wind profile relationship in (13), the height of the jet wind maximum is approximately 0.25D, where D is the valley depth, giving a reference height of 0.05D. Assuming a roughness length of 1 m and a von Kármán constant of 0.35, and using (13) to determine the wind speed at 0.05D, the friction velocity u_* for neutral conditions is

$$u_* = \frac{0.15U_{\text{jet}}}{\ln(0.05D)}, \tag{20}$$

where U_{jet} is the jet wind speed maximum. The vertical eddy diffusivity is then determined as

$$K_z = \frac{0.0175u_*D}{\phi_h}, \tag{21}$$

where the dimensionless temperature gradient ϕ_h is a function of stability and the Monin–Obukhov length, and ϕ_h reduces to constant values of 6 for stable conditions and 0.24 for unstable conditions, assuming that the magnitude of the Monin–Obukhov length always equals the reference height. In summary, K_Z is determined from (21), knowing D and U_{jet}, and the values of ϕ_h, which are 6, 1, and 0.24 for stable, neutral, and unstable conditions, respectively. Friction velocity is actually a function of stability, but for simplicity, the neutral friction velocity from (20) is used in (21) for all stabilities.

The lateral eddy diffusivity K_Y is determined from K_Z as

$$K_Y = \left(\frac{\sigma_v}{\sigma_w}\right)^2 K_Z, \tag{22}$$

where $(\sigma_v/\sigma_w)^2$ is roughly approximated as 5.8 for stable conditions, 2.8 for neutral conditions, and 1.3 for unstable conditions based on observations from the 1984 ASCOT experiments. The values of K_Y and K_Z used in the BCRC valley simulation were 2.55 and 0.44 for stable, 7.38 and 2.64 for neutral, and 14.28 and 10.99 for unstable conditions. The values of D and U_{jet} used to determine the eddy diffusivities were 720 m (the average depth of the valley) and 6 m s^{-1}.

In addition to the model parameters given above, several other parameters were specified for the Brush Creek–Roan Creek valley simulation. The initial concentrations in the computational domain were set to the background PMCH concentration of 1.25×10^{-10} g m^{-3} (0.01 ppt). The boundary condition used in the simulation was of the Dirichlet type, where the inflow concentration is the background concentration. The diffusion through the top boundary of the computational domain can be controlled by multiplying the K_Z in the upper boundary grid cells by a factor of between 0 and 1. A multiplier of 0.1 was used in this simulation. The remaining parameters were $A_0 = 0.3$, $P = 815$ mb, $\rho = 1.0$ kg m^{-3}, $\beta_w = 0.0$ K s^{-1}, $\gamma_\theta = 0.02$ K m^{-1}, and $f_C = 0.15$.

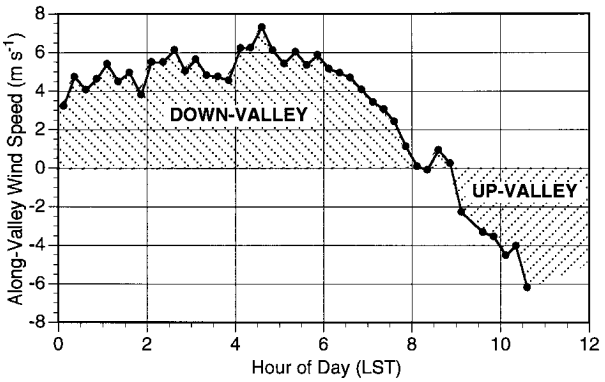

FIG. 6. Fifteen-minute-average along-valley winds at 105 m above the valley floor, determined from sodar observations of wind direction and wind speed.

c. Results and discussion

The along-valley wind speeds at 105 m AGL (height of the jet maximum winds) determined from the Doppler sodar wind speed and direction observations are given in Fig. 6. The down-valley winds slowed after sunrise (0610 LST), eventually switching to up-valley after 0900 LST and increasing to roughly the same speeds (~6 m s^{-1}) as the nighttime down-valley winds.

Time series plots of the 70 observed and predicted PMCH concentrations are given in Fig. 7 for the seven sampler locations identified in Fig. 5. Similarities are evident between the predicted concentrations (upper panel in Fig. 7) and the observed concentrations (lower panel). The nighttime (0100–0700) concentrations predicted at the three sampler locations (B34, B40, and B55) in the Brush Creek valley were approximately equal to the observed concentrations. In fact, the nighttime average predicted concentration of the three samplers agreed to within 10% of the observed average concentration—372 ppt predicted versus 346 ppt observed.

Based on one night of data, Fig. 8 supports the conclusion from Fig. 7 that VALDRIFT has adequately treated the processes governing nighttime dispersion in the Brush Creek valley. The predicted and observed concentrations agreed to within a factor of 1.5, 75% of the time for the nighttime hours at the 3 sampler locations down-valley from the release in the Brush Creek valley.

The predicted and observed nighttime tracer plume arrival times were similar. The plume concentrations are shown in both the upper (predicted) and the lower (observed) panels in Fig. 7 to become nearly steady at 8 km (B34) from the release during the second hour (0100–0200) from the start of the release. VALDRIFT predicted that the plume would reach the B05 sampler

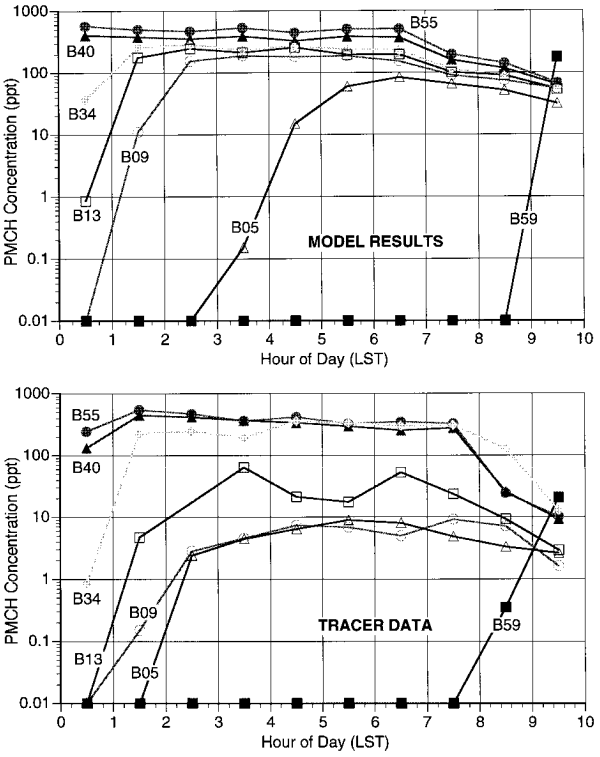

FIG. 7. Predicted (top panel) and observed (bottom panel) PMCH concentrations (ppt) versus time. Ground-level concentrations at the center of the valley are given for seven locations at various distances from the release location.

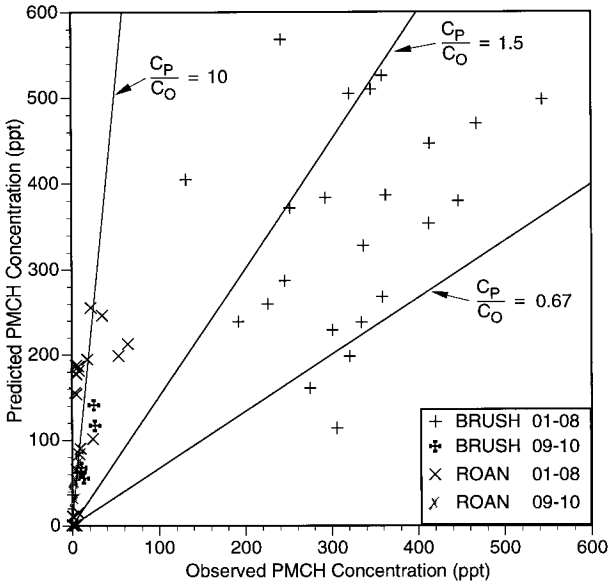

FIG. 8. Predicted versus observed PMCH concentrations (ppt) for the 10 hourly observations at six tracer sampler locations. The 60 data points are plotted as four groups identified in the legend. The BRUSH 01-08 group is the nighttime data (ending times 0100 through 0800) at samplers B34, B40, and B55, located in the Brush Creek valley. The BRUSH 09-10 group is the daytime data (ending times 0900 through 1000) for the same sampler locations as the first group. The ROAN 01-08 group is the nighttime data at samplers B13, B09, and B05, located in the Roan Creek valley, and the ROAN 09-10 group is the daytime data for the same sampler locations. (The lines representing C_p/C_O values of 10, 1.5, and 0.67 are given for illustrative purposes.)

in Roan Creek valley (28 km down-valley from the release point) approximately an hour later than the observed plume arrival time. The actual plume transport speed from the release point to B05 was about 2.5 m s^{-1} (28 km/3 h) versus about 2 m s^{-1} (28 km/4 h) for the model prediction. The underprediction of the plume transport speed was evidently caused by not including the new air mass from the Roan Creek valley, which enters the computational domain at the Brush Creek–Roan Creek merger. The importance of these merging tributary flows on the behavior of the tracer plume will become more evident in the following discussion.

The nighttime concentrations predicted by VALDRIFT at the three sampler locations (B13, B09, and B05) in the Roan Creek valley were, on the average, a factor of 9 greater than the observed concentrations (128-ppt average predicted concentration versus 14-ppt average observed concentration). A point-to-point comparison of predicted versus observed concentrations in Fig. 8 shows the general overprediction of the tracer concentrations in the Roan Creek valley. This difference between the predicted and observed nighttime concentrations demonstrates the importance of the merging airstreams on tracer plume dispersion and provides valuable guidance for the future parameterization of the merging process.

Volume dilution and increased turbulence are the likely causes of the enhanced nighttime tracer plume dispersion resulting from the merging of the Brush Creek and Roan Creek valley flows. Estimates of air volume flow from the Roan Creek valley support a factor of 2–3 reduction of tracer concentrations that would result when clean air from the Roan Creek valley dilutes the tracer-laden air from the Brush Creek valley. This volume dilution process, however, does not account for the factor of 9 difference between the model and the observations. Enhanced turbulence likely accounts for the remaining difference. The level of turbulence in the valley air after the two airstreams merge is undoubtedly much greater than the turbulence just upstream in Brush Creek valley. Turbulent eddies comparable in size to the plume dimensions will be present, effectively breaking apart the plume.

After sunrise (0610 LST), the convective boundary layer begins growing and the top of the nocturnal temperature inversion begins descending, as illustrated in Fig. 9. VALDRIFT predicted the nocturnal temperature inversion to be fully destroyed by 1100 LST. Also shown in Fig. 9 are the turbulent eddy diffusivities used as a function of height above the valley floor and time of day. The vertical diffusivity in the CBL was 25 times greater than K_Z in the stable core. The predicted concentrations in Fig. 7 at the 6 sampler locations down-

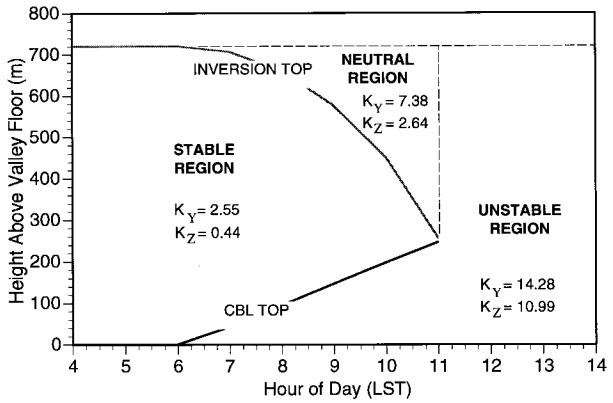

FIG. 9. Inversion-top height and CBL-top height versus time for the Brush Creek valley simulation. The turbulent eddy diffusivities K_Y and K_Z are in units of square meters per second.

valley from the release point decreased after sunrise, demonstrating the effect of the enhanced diffusion in the CBL.

After the down-valley winds reversed at 0830–0900 LST, the much lower tracer concentrations from the Roan Creek valley, which were caused by dilution and enhanced turbulence, simply advected up-valley past the samplers in Brush Creek valley, resulting in much lower tracer concentrations than VALDRIFT predicted and would be expected by diffusion alone (Allwine 1993). The flow reversal is indicated in Fig. 7 by the increase in predicted and observed tracer concentration at sampling point B59, which is located up-valley from the release point. All the daytime points in Fig. 8 fall near the $C_p/C_O = 10$ line because of the residual effect of the nighttime merged flows.

4. Summary and conclusions

VALDRIFT treats the transport, diffusion, and deposition of an inert substance released from multiple point and/or line sources in a valley atmosphere, where the sources may be elevated or at ground level, and the release rate from each source can vary with time. VALDRIFT is configured to operate through one diurnal cycle for a single mountain valley having relatively steep sidewalls. The inputs required are the valley topographic characteristics, the pollutant release rate as a function of time and space, wind speed and direction as functions of time measured at one height, lateral and vertical turbulent eddy diffusivities as functions of stability, and the valley temperature inversion characteristics at sunrise. The outputs are three-dimensional concentration fields and ground-level deposition fields as functions of time.

VALDRIFT is a phenomenological model in which the dominant meteorological processes governing the behavior of the valley atmosphere are formulated explicitly in the model, although in a highly parameterized fashion. The physical processes currently treated explicitly are nonsteady and nonhomogeneous along-valley winds and turbulent diffusivities, convective boundary layer growth, inversion descent, and nocturnal temperature inversion breakup. Slope flows, cross-valley circulations, interactions with above-ridge-top winds, subsidence, nocturnal temperature inversion formation, and tributary flows are not currently treated in VALDRIFT.

The VALDRIFT model reasonably reproduced ground-level tracer concentrations measured during a 26 September 1984 experiment conducted in Colorado's 700–900-m-deep Brush Creek–Roan Creek valley system. The nighttime concentrations predicted by VALDRIFT at the three sampler locations in the Brush Creek valley agreed to within 10% of the observed average concentration. The modeled and observed arrival times of the nighttime tracer plume agreed to within 1 h at each of the three tracer sampling sites. The nighttime concentrations predicted by VALDRIFT at the three sampler locations in the Roan Creek valley were, on average, nine times greater than the observed concentrations. This overprediction demonstrates the importance of clean tributary flows on tracer plume dispersion. Dilution of the Brush Creek valley tracer plume with clean air from the upper Roan Creek valley and increased turbulence in the merging flows are the likely causes for the enhanced dispersion. VALDRIFT predicted that the daytime concentrations in the Brush Creek valley would decrease at a slower rate than the observed concentrations because the model advected higher concentrations up-valley into Brush Creek valley after wind reversal.

Applying VALDRIFT to the Brush Creek–Roan Creek valley system has allowed the effect of merging tributaries to be quantified and provides valuable guidance for the future parameterization of these processes. The VALDRIFT model should be enhanced to treat tributary flows in addition to cross-valley circulations. Incorporating these changes will allow VALDRIFT to be applied to systems of valleys, to broader valleys, and over a wider range of meteorological conditions, such as cloudy periods and times of strong synoptic winds.

Acknowledgments. The authors would like to thank Mr. Robert Ekblad, the Forest Service project manager during the earlier phases of this work, for funding, encouragement, and suggestions. The authors would also like to thank Mr. Jack Barry of the FS Forest Health Technology Enterprise Team for his support of this work. This work was supported by the U.S. Department of Agriculture Forest Service under a Related Services Agreement with the U.S. Department of Energy under Contract DE-AC06-76RLO 1830, Interagency Agreement 5E52P29. Pacific Northwest National Laboratory is operated for DOE by Battelle Memorial Institute. The FS provided partial support to one of the authors (KJA) for preparation of this paper through a contract with Allwine Environmental Services.

REFERENCES

Allwine, K. J., 1992: Atmospheric dispersion in mountain valleys and basins. PNL-7922, 207 pp. [Available from Pacific Northwest National Laboratory, P. O. Box 999, Richland, WA 99352.]

——, 1993: Atmospheric dispersion and tracer ventilation in a deep mountain valley. *J. Appl. Meteor.,* **32,** 1017–1037.

——, X. Bian, and C. D. Whiteman, 1995: VALDRIFT 1.0—A valley atmospheric dispersion model with deposition. PNL-10586, 136 pp. [Available from Pacific Northwest National Laboratory, P. O. Box 999, Richland, WA 99352.]

Bader, D. C., and T. B. McKee, 1985: Effects of shear, stability and valley characteristics on the destruction of temperature inversions. *J. Climate Appl. Meteor.,* **24,** 822–832.

——, and C. D. Whiteman, 1989: Numerical simulation of cross-valley plume dispersion during the morning transition period. *J. Appl. Meteor.,* **28,** 652–664.

Bilanin, A. J., M. E. Teske, J. W. Barry, and R. B. Ekblad, 1989: AGDISP: The aircraft spray dispersion model, code development and experimental validation. *Trans. ASAE,* **32,** 327–334.

Businger, J. A., J. C. Wyngaard, Y. Izumi, and E. F. Bradley, 1971: Flux profile relations in the atmospheric surface layer. *J. Atmos. Sci.,* **28,** 181–189.

Clements, W. E., J. A. Archuleta, and P. H. Gudiksen, 1989a: Experimental design of the 1984 ASCOT field study. *J. Appl. Meteor.,* **28,** 405–413.

——, ——, and D. E. Hoard, 1989b: Mean structure of the nocturnal drainage flow in a deep valley. *J. Appl. Meteor.,* **28,** 457–462.

Doran, J. C., T. W. Horst, and C. D. Whiteman, 1990: The development and structure of nocturnal slope winds in a simple valley. *Bound.-Layer Meteor.,* **52,** 41–68.

Ekblad, R. B., and J. W. Barry, 1990: Selection and verification of complex terrain wind flow model for spray transport—Briefing paper and progress report. USDA Forest Service Rep. 5E52P29 WIND, 100 pp. [Available from Missoula Technology Development Center, Fort Missoula, Building 1, Missoula, MT 59801.]

——, C. D. Whiteman, K. J. Allwine, and J. W. Barry, 1991: Wind flow model for spray transport in complex terrain. *1991 Proc. Int. Summer Meeting of the American Society of Agricultural Engineers,* Albuquerque, NM, ASAE, 1–13.

Gryning, S.-E., and E. Lyck, 1983: A tracer investigation of the atmospheric dispersion in the Drynaes Valley, Greenland. RISO-R-481, 67 pp. [Available from RISO National Laboratory, DK-4000 Roskilde, Denmark.]

Gudiksen, P. H., G. J. Ferber, M. M. Fowler, W. L. Eberhard, M. A. Fosberg, and W. R. Knuth, 1984: Field studies of transport and dispersion of atmospheric tracers in nocturnal drainage flows. *Atmos. Environ.,* **18,** 713–732.

Hanna, S. R., G. A. Briggs, and R. P. Hosker, 1982: Handbook on atmospheric diffusion. DOETIC-11223, 102 pp. [NTIS DE82 002 045.]

Hewson, E. W., and G. C. Gill, 1944: Meteorological investigations in Columbia River valley near Trail, B.C. *Bur. Mines Bull.,* **453,** 23–228.

McNider, R. T., 1981: Investigation of the impact of topographic circulations on the transport and dispersion of air pollutants. Ph.D. dissertation, University of Virginia, 185 pp. [Available from University Microfilms, 300 Zeeb Road, Ann Arbor, MI 48106.]

Panofsky, H. A., and J. A. Dutton, 1984: *Atmospheric Turbulence, Models and Methods for Engineering Applications.* John Wiley and Sons, 397 pp.

Segal, M., C. H. Yu, R. W. Arritt, and R. A. Pielke, 1988: On the impact of valley/ridge thermally induced circulations on regional pollutant transport. *Atmos. Environ.,* **22,** 471–486.

Start, G. E., C. R. Dickson, and L. L. Wendell, 1975: Diffusion in a canyon within rough mountainous terrain. *J. Appl. Meteor.,* **14,** 333–346.

Teske, M. E., J. F. Bowers, J. E. Rafferty, and John W. Barry, 1993: FSCBG: An aerial spray dispersion model for predicting the fate of released material behind aircraft. *Environ. Toxicol. Chem.,* **12,** 453–464.

Tyson, P. D., 1969: Air pollution fumigation conditions associated with the dissipation of the mountain wind and onset of the valley wind over Pietermaritzburg. *South. Afr. Geogr. J.,* **51,** 99–105.

Vergeiner, I., E. Dreiseitl, and C. D. Whiteman, 1987: Dynamics of katabatic winds in Colorado's Brush Creek valley. *J. Atmos. Sci.,* **44,** 148–157.

Wanner, H., and J. Hertig, 1984: Studies of urban climates and air pollution in Switzerland. *J. Climate Appl. Meteor.,* **23,** 1614–1625.

Whiteman, C. D., 1989: Morning transition tracer experiments in a deep narrow valley. *J. Appl. Meteor.,* **28,** 626–635.

——, 1990: Effects of valley meteorology on forest pesticide spraying. PNL-7332, 19 pp. [Available from Pacific Northwest National Laboratory, P. O. Box 999, Richland, WA 99352.]

——, and T. B. McKee, 1982: Breakup of temperature inversions in deep mountain valleys: Part II. Thermodynamic model. *J. Appl. Meteor.,* **21,** 290–302.

——, and K. J. Allwine, 1985: VALMET—A valley air pollution model. PNL-4728 Rev. 1, 190 pp. [Available from Pacific Northwest National Laboratory, P. O. Box 999, Richland, WA 99352.]

——, and ——, 1986: Extraterrestrial solar radiation on inclined surfaces. *Environ. Software,* **1,** 164–169.

Willson, R., F. Shair, B. Reynolds, and W. Greene, 1983: Characterization of the transport and diffusion of pollutants in a narrow mountain valley region by means of an atmospheric tracer. *Atmos. Environ.,* **17,** 1633–1647.